NRL Report 6861

Ionosphere Propagation Delay Measurement Techniques Using Dual Phase Coherent Doppler Frequencies And a Thin Shell Model

G. PAUL LANDIS AND LOUIS D. BREETZ

Space Applications Branch
Applications Research Division

April 8, 1969

Naval Research Laboratory
Washington, D.C.

This document has been approved for release and sale; its distribution is unlimited

CONTENTS

Abstract	ii
Problem Status	ii
Authorization	ii
INTRODUCTION	1
IONOSPHERIC DELAY	1
SUPPORTING EQUIPMENT	6
DATA REDUCTION	8
EXPERIMENTAL RESULTS	9
REFERENCES	12
APPENDIX A — Calculations of Range Error by the Low-Angle and High-Angle Methods	13

ABSTRACT

A theoretical approach was made to developing a technique for approximating the time error of a signal from a satellite caused by free electrons reducing the electromagnetic propagation speed. The development involved the use of the Transit satellites' dual frequency transmissions at 400 and 150 MHz, the AN/SRN-9 receiver, and a knowledge of the orbital location of the satellite. The technique gives a reasonably close delay measurement for a given satellite at a given time under a given ionospheric condition.

PROBLEM STATUS

This is an interim report on a continuing problem.

AUTHORIZATION

NRL Problem R04-16
Project A37-538-002/652-1/F019-01-01

Manuscript submitted November 21, 1968.

IONOSPHERE PROPAGATION DELAY MEASUREMENT TECHNIQUES USING DUAL PHASE COHERENT DOPPLER FREQUENCIES AND A THIN SHELL MODEL

INTRODUCTION

The free electron content of the ionosphere causes electromagnetic radiation to propagate at a reduced speed. This change in propagation-velocity introduces a time error when a transmitted signal from a space orbiting satellite is used as a time transfer or a navigational device.

Through the use of the Transit satellites' dual frequency transmissions at 400 and 150 MHz, the AN/SRN-9 receiver, and a knowledge of the orbital location of the satellite, a technique was developed to approximate the error due to ionospheric irregularities.

IONOSPHERIC DELAY

The velocity of propagation is inversely proportional to the square root of the dielectric constant. The dielectric constant of the ionosphere with its free electrons in the earth's magnetic field is a complex tensor. However, if the magnetic field is neglected, we may assume an isotropic dielectric constant (1).

The magnitude of the ratio between the propagation velocity in the ionosphere (V_2) to that in a vacuum (V_1) is very nearly 1. The Snell law states that $V_2/V_1 = \cos\theta_1/\cos\theta_2$, where θ_1 and θ_2 are the angles the respective wave propagation paths make with the boundary surface. The difference ($\Delta\theta = \theta_1 - \theta_2$) in the angles of the waves in the two mediums is small. The additional path length produced by this bending is approximately ($1 - \cos\Delta\theta$) times the original length. Willman and Tucker (2) found that a 54-MHz ray through a layer at a height of 625 km and an elevation angle of 41.29° deviated about 3926 m from a straight-line path and that the ray through another layer 165 km in height and a small elevation angle of 0.81° deviated 82.05 km. This would amount to an additional path length of under 20 m for the 41° source and under 5 km for the 0.81° source. The bending is less as the elevation angle is greater. The bending decreases further with a frequency increase approximately proportional to $1/f$. The delay is proportional to $1/f^2$. If the delays for the 5-km and 20-m additional path lengths at 54 MHz are projected to 400 MHz, the delays would be that which would result from path lengths of less than 100 m and 1 m.

The delay due to path length change will be shown to be a second-order delay compared to that produced by a velocity of propagation change along the straight path in the medium.

The ionospheric delay expressed in distance can be shown to be equal to

$$\Delta L = \frac{b}{\omega^2} \int_{\text{transmitter}}^{\text{receiver}} N(s)\, ds \,, \tag{1}$$

where s is assumed to be a straight-line path, $N(s)$ is the electron density per unit volume, ω is the angular frequency (rad/sec), and b is a constant equal to $e^2/2\epsilon_0 m$, in which e is the charge of an electron, ϵ_0 is the electric permittivity of free space, and m is the mass of an electron.

The $1/\omega^2$ term is a first-order approximation for the frequency dependence of the delay. The errors introduced by the $1/\omega^2$ approximation can be of the order of 9% for angles near the horizon and zero at the angles of closest approach (2).

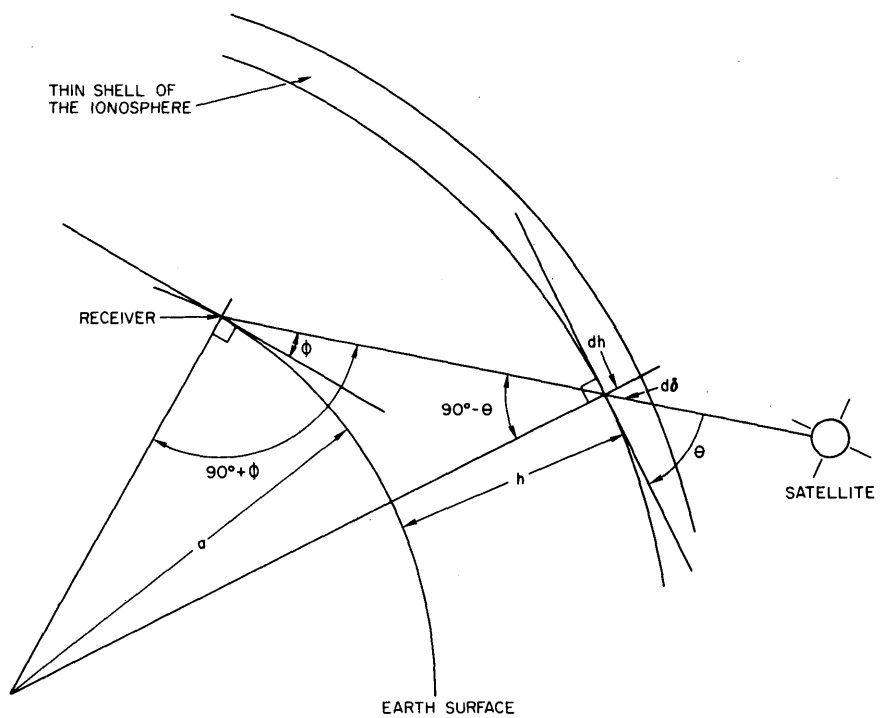

Fig. 1 - Obliquity factor geometry used to transform the path length through an ionosphere shell ds into a function of elevation angle ϕ, shell altitude h, and thickness dh (taken from Fig. 6-12 of Ref. 3a)

Referring to Fig. 1 showing the earth and incremental shell surrounding the portion of earth shown, where a is the earth's radius, h is the height of shell above earth, ϕ is the angle the transmitted wave makes with the tangent to the earth at the receiver point, and θ is the angle between the transmitted wave and tangent to the shell, Eq. (1) gives

$$\Delta L = \frac{b}{\omega^2} \int_{h_t}^{h_r} \frac{N(h,\phi)\, dh}{\sin\theta} = \frac{b}{\omega^2} \int_{h_t}^{h_r} N(h,\phi)\, Q(h,\phi)\, dh ,$$

where $Q(h,\phi) = 1/\sin\theta$ is the obliquity factor.

Actually $N(s)$ in Eq. (1) is also a function of the time and azimuth-angle variables. By working with half of a pass it can be shown that time, altitude, elevation angle, and azimuth angle are single valued and dependent functions.

By the law of sines,

$$\frac{\sin\left(\frac{\pi}{2} - \theta\right)}{a} = \frac{\sin\left(\frac{\pi}{2} + \phi\right)}{a + h}$$

or

$$\cos\theta = \frac{a}{a + h}\cos\phi ,$$

so that

$$Q(h,\phi) = \frac{1}{\sin\theta} = \left[1 - \left(\frac{a}{a + h}\right)^2 \cos^2\phi\right]^{-1/2} \tag{2}$$

and

$$\Delta L = \frac{b}{\omega^2}\int_{h_t}^{h_r} \frac{N(h,\phi)}{\left[1 - \left(\frac{a}{a + h}\right)^2 \cos^2\phi\right]^{1/2}}\, dh .$$

The vertical dependence of $N(h,\phi)$ is approximately as shown in the typical electron density profile of Fig. 2. The peak may vary from 200 to 500 km and the base from 80 to 100 km.

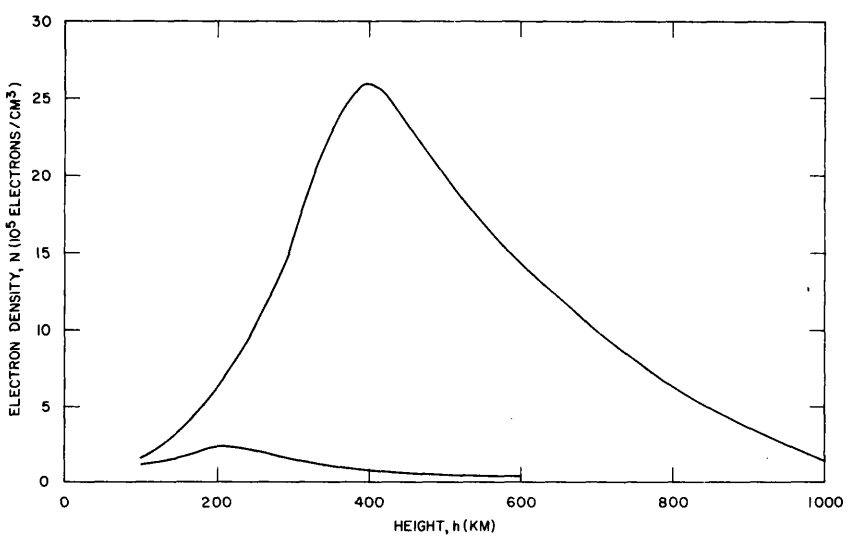

Fig. 2 - The two extremes of a typical range of electron density $N(h)$ vs altitude h (data from Fig. 6-13 of Ref. 3a)

The function $Q(h,\phi)$ for angles above 15° and for a typical value of h has a small fractional change with h. The integral for ΔL can be approximated by defining

$$Q(h,\phi) = Q(\bar{h},\phi)$$

where $\bar{h}$ is the altitude of the peak of the electron density. This is called the thin-shell approximation, because it is equivalent to assuming that all the electrons are concentrated in a layer at the altitude $\bar{h}$. Thus

$$\Delta L = \frac{b}{\omega^2} Q(\bar{h},\phi) \int_{h_t}^{h_r} N(h,\phi)\, dh = \frac{bN_T}{\omega^2} Q(\bar{h},\phi) \ , \tag{3}$$

where N_T is the total number of electrons in a vertical column of unit area between the altitude of the transmitter and the altitude of the receiver.

Using this thin shell approximation with only a knowledge of N_T and $\bar{h}$, ΔL values will be within ±10% when ϕ is greater than 15° (3b).

It will be shown later that data coming from the receiver is in the form of rate of change of path length with respect to time. To keep these variables the same as in the delay equation, $d(\Delta L)/d\phi$ is evaluated, where $\phi = f(t)$ is known:

$$\frac{d(\Delta L)}{d\phi} = \frac{b}{\omega^2} \left\{ \int_{h_t}^{h_r} \frac{\partial}{\partial \phi} \left[N(h,\phi)\, Q(h,\phi) \right] dh \right.$$

$$\left. + N(h_r,\phi)\, Q(h_r,\phi) \frac{dh_r}{d\phi} - N(h_t,\phi)\, Q(h_t,\phi) \frac{dh_t}{d\phi} \right\} .$$

But since the electron density at the receiver happens to be zero, $N(h_r,\phi) = 0$, and since the receiver is fixed in position, $dh_r/d\phi = 0$, so that

$$\frac{d(\Delta L)}{d\phi} = \frac{b}{\omega^2} \left[\int_{h_t}^{h_r} Q(h,\phi) \frac{\partial N(h,\phi)}{\partial \phi}\, dh + \int_{h_t}^{h_r} N(h,\phi) \frac{\partial Q(h,\phi)}{\partial \phi}\, dh - N(h_t,\phi)\, Q(h_t,\phi) \frac{dh_t}{d\phi} \right] \tag{4}$$

Evaluation of the first term within the brackets of Eq. (4) using the thin-shell concept, where $Q(h,\phi) = Q(\bar{h},\phi)$, gives

$$\int_{h_t}^{h_r} Q(h,\phi) \frac{\partial N(h,\phi)}{\partial \phi}\, dh = Q(\bar{h},\phi) \int_{h_t}^{h_r} \frac{\partial N(h,\phi)}{\partial \phi}\, dh \ . \tag{5}$$

Expansion of the integral gives

$$\int_{h_t}^{h_r} \frac{\partial N(h,\phi)}{\partial \phi}\, dh = \frac{d}{d\phi} \int_{h_t}^{h_r} N(h,\phi)\, dh - N(h_r,\phi) \frac{dh_r}{d\phi} + N(h_t,\phi) \frac{dh_t}{d\phi} \ ,$$

and again $N(h_r,\phi) = 0$, $dh_r/d\phi = 0$, and

$$\int_{h_t}^{h_r} N(h,\phi) = N_T \ ,$$

so that

$$\int_{h_t}^{h_r} \frac{\partial N(h,\phi)}{\partial \phi}\, dh = \frac{dN_T}{d\phi} + N(h_t,\phi) \frac{dh_t}{d\phi} \ .$$

Hence Eq. (5) may be written

$$\int_{h_t}^{h_r} Q(h,\phi)\frac{\partial N(h,\phi)}{d\phi}\,dh = Q(\bar{h},\phi)\left(\frac{dN_T}{d\phi} + N(h_t,\phi)\frac{dh_t}{d\phi}\right).$$

Evaluation of the second term within the brackets of Eq. (4) gives

$$\int_{h_t}^{h_r} N(h,\phi)\frac{\partial Q(h,\phi)}{\partial\phi}\,dh = -\frac{1}{2}\sin 2\phi\int_{h_t}^{h_r} N(h,\phi)\left(\frac{a}{a+h}\right)^2 Q^3(h,\phi)\,dh\,, \tag{6}$$

since

$$Q = \left[1 - \left(\frac{a}{a+h}\right)^2\cos^2\phi\right]^{-1/2}$$

and

$$\frac{dQ}{d\phi} = -\frac{1}{2}\left(\frac{a}{a+h}\right)^2 \sin 2\phi\, Q^3(h,\phi)\,.$$

Under the thin shell approximation where $a/(a+h) = a/(a+\bar{h})$, $Q(h,\phi) = Q(\bar{h},\phi)$, and

$$\int_{h_t}^{h_r} N(h,\phi)\,dh = N_T\,,$$

Eq. (6) becomes

$$\int_{h_t}^{h_r} N(h,\phi)\frac{\partial Q(h,\phi)}{\partial\phi}\,dh = -\frac{1}{2}\sin 2\phi\left(\frac{a}{a+\bar{h}}\right)^2 Q^3(\bar{h},\phi)\,N_T = \frac{dQ(\bar{h},\phi)}{d\phi}\,N_T\,.$$

This use of the thin shell approximation will probably have several times the error over its use in the evaluation of ΔL (Eq. (3)):

$$\frac{d(\Delta L)}{d\phi} = \frac{b}{\omega^2}\left\{N(h_t,\phi)\frac{dh_t}{d\phi}\left[Q(\bar{h},\phi) - Q(h_t,\phi)\right] + Q(\bar{h},\phi)\frac{dN_T}{d\phi} + N_T\frac{dQ(\bar{h},\phi)}{d\phi}\right\}.$$

The first term, $(b/\omega^2)\,N(h_t,\phi)\,dh_t/d\phi\,[Q(\bar{h},\phi) - Q(h_t,\phi)]$, is proportional to the electron density at the satellite $N(h_t,\phi)$, the rate of change of the altitude of the satellite with respect to angle $dh_T/d\phi$, and the difference in obliquity factor at $\bar{h}$ and h_t: $Q(\bar{h},\phi) - Q(h_t,\phi)$. The second term, $(b/\omega^2)\,Q(h,\phi)\,dN_T/d\phi$, is due to horizontal gradients and time changes. The third term, $(b/\omega^2)\,N_T\,dQ(\bar{h},\phi)/d\phi$, is what would have been obtained if the derivative of Eq. (3) had been taken.

In the approximate evaluation of these terms, $Q(\bar{h},\phi)$ and $Q(h_t,\phi)$ will be assumed to have a maximum value of 1.5 because of the value of $\bar{h}$ and h_t and the elevation angle restrictions, $\phi > 15°$, imposed by the use of the thin shell model. Their difference will be assumed to have a maximum value of 0.5.

$N(h_t, \phi)$, at 1000 km, has a maximum value of about 2×10^{11} electrons/m^3 (3c). The value of N_T is about 10^{18} electrons/m^2 to an altitude of 1000 km and can change by a factor of 10 in each direction (3d). If it is assumed that $N(h_t, \phi)$ is proportional to N_T, the maximum values give

$$N(h_t, \phi) = \frac{2 \times 10^{-7}}{\text{meter}} N_T .$$

Through a change of form $d(\Delta L)/d\phi$ becomes

$$\frac{d(\Delta L)}{d\phi} = \frac{bN_T}{\omega^2} \left\{ \frac{dt}{d\phi} \left[\frac{1}{2} \frac{2 \times 10^{-7}}{\text{meter}} \frac{dh_t}{dt} + \frac{1.5}{N_T} \left(\frac{dN_T}{dt} + \frac{dN_T}{dt} + \frac{dN_T}{ds} \frac{ds}{dt} \right) \right] + \frac{dQ}{d\phi} (\bar{h}, \phi) \right\} .$$

The orbit of the satellite is such that $dh_t/dt \approx 2 \times 10^3$ m/min. Also since dN_T/dt is about equal to 1% N_T per 200 sec or $dN_T/N_T dt = 3 \times 10^{-3}$ per min, and since dN_T/ds = 1% N_T per 100 km (4), and since $ds/dt \approx (\bar{h}/h_t)$ 440 km/min (based on the orbit), then

$$1/N_T \left(\frac{dN_T}{dt} + \frac{dN_T}{ds} \frac{ds}{dt} \right) = (1.5 \times 10^{-2} + 3 \times 10^{-3}) \text{ per min} \approx 1.5 \times 10^{-2} \text{ per min.}$$

Considering the largest terms in the approximation, $d(\Delta L)/d\phi$ becomes

$$\frac{d(\Delta L)}{d\phi} \approx \frac{bN_T}{\omega^2} \left[\frac{dt}{d\phi} \frac{2.25 \times 10^{-2}}{\text{min}} + \frac{dQ}{d\phi} (\bar{h}, \phi) \right] .$$

In the range ϕ = 10° to 15°, $|dQ/d\phi|$ is near or at its maximum value for a reasonable range of $\bar{h}$, but the thin shell approximation leaves much to be desired in this range.

A rough approximation above 30° that improves with elevation is $Q = \csc \phi$ (3e), giving $dQ/d\phi = -\csc \phi \cot \phi$. The value of $dt/d\phi$ is a function of the orbit and goes to infinity at closest approach. With the satellite passes used to obtain experimental data the minimum values for $dt/d\phi$ occurred at angles around 0.8 to 0.9 of the maximum elevation angle of ϕ and have an approximate value of 4 to 6 min per ϕ max.

Using the values of $dt/d\phi$ and $dQ/d\phi$ it is found for angles between about 15° and 0.8 or 0.9 of ϕ max that the contribution to $\partial(\Delta L)/d\phi$ from changes in satellite altitude, horizontal gradients, and time change in electron density amount to only 5 to 10% of the total. Therefore assuming

$$\frac{d(\Delta L)}{d\phi} \approx \frac{bN_T}{\omega^2} \frac{dQ}{d\phi} (\bar{h}, \phi)$$

the largest error in the expression is from the thin shell approximation used in the term that gives $dQ(\bar{h}, \phi)/d\phi$.

SUPPORTING EQUIPMENT

The primary equipment was an SRN-9 navigation receiver which was used to track four doppler satellites. The satellites transmit at 149.988 MHz and 399.968 MHz (nominally 150 and 400 MHz) and are exactly in the ratio of 3:8. The received signal is shifted in frequency by doppler and ionospheric effects.

The received frequency f_r and the transmitted frequency f_t are related by $f_r = f_t [1 - (1/c)\, ds/dt]$, in which c is the velocity of propagation in a vacuum and $s = L + \Delta L$ is the total path length from the receiver to the satellite, where L is the straight-line length and ΔL is the equivalent ionospheric delay in distance. The received frequencies from the 150-MHz and 400-MHz satellite transmitters would be

$$f_{r_{150}} = f_{t_{150}} \left[1 - \frac{1}{c} \left(\frac{dL}{dt} + \frac{d\,\Delta L_{150}}{dt} \right) \right]$$

and

$$f_{r_{400}} = f_{t_{400}} \left[1 - \frac{1}{c} \left(\frac{dL}{dt} + \frac{d\,\Delta L_{400}}{dt} \right) \right] .$$

The receiver processes the two received frequencies in the following manner. The 400-MHz signal is multiplied by a factor of 3/8 and then mixed with the 150-MHz signal so that the mixer output frequency is

$$f_{mix} = 3/8\ f_{r_{400}} - f_{r_{150}}$$

But the mixed frequency of the 400-MHz and 150-MHz signals modified by the doppler and ionosphere is

$$f_{mix} = \frac{3}{8}\ f_{t_{400}} \left[\frac{1}{c} \left(\frac{d\Delta L_{150}}{dt} - \frac{d\Delta L_{400}}{dt} \right) \right]$$

Assuming $\Delta L_{150} = (8/3)^2\, \Delta L_{400}$, since the ionospheric delay is approximately inversely proportional to the frequency squared,

$$f_{mix} = \frac{3}{8} \frac{1}{\lambda_{400}} \frac{55}{9} \frac{d\Delta L_{400}}{dt}$$

and

$$\frac{d\Delta L_{400}}{dt} = f_{mix} \frac{24}{55} \lambda_{400} = f_{mix} \frac{1.0737\ ft}{cycle} = f_{mix} \frac{0.3273\ meters}{cycle} \tag{7}$$

or

$$d\Delta L_{400} = f_{mix}\ (1.0737\ \text{ft/cycle})\ dt$$

and

$$d\Delta L_{150} = f_{mix}\ (7.6352\ \text{ft/cycle})\ dt .$$

The $d\Delta L_{400}/dt$ of Eq. (7) can be either positive or negative, and this information is obtained from the SRN-9 by having two mixers with a quadrature network on the input to one mixer. The quadrature relationship of the mixer outputs indicates the sign of $d\Delta L\ dt$.

To aid in the processing of the receiver output data, additional electronic equipment was utilized. Since the quadrature outputs of the two mixers have a maximum frequency near 8 Hz, it was possible to display the outputs on an oscilloscope as a Lissajou figure. The sign of $d\Delta L/dt$ can be determined by the direction of rotation of the dot on the scope. The noise in the signal is indicated by the irregularity in the circular motion of the dot.

The purpose of the study was to measure ionospheric path length rather than rate of change. The integration of $d\Delta L/dt$ was done easily by electronic counters. Two ungated counters were used with the signal being switched between them, depending on the sign of $d\Delta L/dt$ as indicated by the dot movement of the Lissajou figure. Changes in the difference in the count of the counters are proportional to changes in the path length through the ionosphere. An integration constant exists that will be evaluated in the next section.

The outputs of the counters were displayed in the form of a staircase signal on a chart recorder with the receiver agc voltages, quadrature outputs of the mixers, and a time coded signal. In addition, the outputs of the counters were connected to two digital-to-analog (D-A) converters. The D-A converter outputs were, in turn, used to drive differential inputs of a second recorder to show the integrated count from the frequency mixer against time.

DATA REDUCTION

Two methods will be derived to calculate the integration constant: one method for data at low angles such as between 25° and 30° and the other method for high angles between 45° and 0.8 ϕ_{max}. Both methods use the approximation $d(\Delta L)/d\phi = (bN_T/\omega^2)(dQ/d\phi)$.

For the low-angle method the ratio was taken of $d(\Delta L)/d\phi$ for two angles:

$$K = \frac{d(\Delta L)/d\phi]_{\phi_1}}{d(\Delta L)/d\phi]_{\phi_2}} = \frac{\sin 2\phi_1}{\sin 2\phi_2} \frac{\left[1 - (a/a+h)^2 \cos^2 \phi_2\right]^{3/2}}{\left[1 - (a/a+h)^2 \cos^2 \phi_1\right]^{3/2}} .$$

Since the magnitude and sign of errors of $d(\Delta L)/d\phi$ at ϕ_1 and ϕ_2 are nearly the same, there will be a reduction in the errors of K as compared with those of $d(\Delta L)/d\phi$. Curves of the K function which uniquely define a value of h for a given ratio have been made to facilitate easy data processing. Since h and ϕ give a value for Q (defined in Eq. (2)), N_T or $N_T b/\omega^2$ can be found from

$$\Delta L_1 - \Delta L_2 = \frac{N_T b}{\omega^2}(Q_1 - Q_2) ,$$

completely solving the equation for ΔL. For convenience $Q_1 - Q_2$ was available from prepared plots of $Q_1 - Q_2$ vs K. The curves were also drawn for elevation angles of $\phi_1 = 25°$ and $\phi_2 = 30°$ for measuring Q. These angles were chosen high enough to satisfy the ray-bending approximation, the thin shell approximation, and the inverse square approximation. Choice of higher angles would have reduced the usefulness and accuracy of the curves, because the ratio of the slopes K is less at higher angle values. At higher angles the receiver monopole antenna pattern causes the signal strength to diminish, resulting in the receiver losing lock as the satellite approaches 90° elevation angle. The two angles were also chosen with a 5° difference as a compromise to obtain better data by providing an ample length of time but short enough to minimize the horizontal and time variable gradients in the ionosphere.

Predictions were obtained to give the elevation angle to the satellite every minute during a pass (5). By assuming a linear approximation between the minute time durations, the time that the satellite is at a given angle can be determined to a fraction of a second.

Data (the difference in cycle count) were taken between the angles of 22.5° and 27.5° and between the angles of 27.5° and 32.5°. These data were used to construct a parabola of count vs angle. It can be shown for this curve that the slope at the 25° and 30° angles, chosen for the set of prepared working curves for $Q_1 - Q_2$ vs K, is equal to the average slope between 22.5° and 27.5° and between 27.5° and 32.5° and the difference between the count at 25° and 30° is equal to one half the difference between the count at 22.5° and 32.5°.

The high-angle method is much simpler and makes use of the approximation $Q = \csc \phi$, which is a very good approximation above $\phi = 45°$:

$$\frac{d(\Delta L)}{d\phi} = \frac{N_T b}{\omega^2} \frac{dQ}{d\phi} = \frac{-N_T b}{\omega^2} \cot \phi \csc \phi ,$$

so that

$$\Delta L = \frac{N_T b}{\omega^2} Q = \frac{-1}{\cot \phi \csc \phi} \frac{d(\Delta L)}{d\phi} \csc \phi$$

or

$$\Delta L = -\tan \phi \frac{d(\Delta L)}{d\phi} .$$

This method can be used between 45° and 0.8 ϕ_{max}. By taking the change in count over a period of time derived from the data and dividing it by the change in angle in radians over the same period of time, $d(\Delta L)/d\phi$ is found.

A comparison between satellite rise and set data shows a dissymmetry of delay about the angle of closest approach, since this rarely coincides with the region of highest electron content. In nearly all cases the highest electron content is south of the closest approach (for the north temperate zone location). The difference in ionosphere delay is comparable to the difference in cycle count. The largest difference between rise and set count has been around 200 ft at 400 MHz. Inaccuracies in determining this difference are caused by such things as the receiver losing lock, causing error in the count, and incorrect angle-to-time transformation based on orbital predictions, causing error in the count and the slope. Other inaccuracies may be attributed to thin shell approximations and the effects of a horizontal gradient of the ionosphere and how it varies during the period of measurement.

Due to unknown ionospheric changes during the measurement period it is impossible to write exact expressions and integrate ΔL precisely. For this reason the assumed values were often considered to be constant during the measuring period. However, by accepting the reasonably close assumptions used in the two methods of measurement, fairly accurate values of ΔL may be obtained.

An appendix provides sample calculations based on the above methods. Included are samples of the helpful work-saving charts and graphs used.

EXPERIMENTAL RESULTS

Measurement of differences in radio propagational vs geometrical path lengths between this Laboratory's location and Transit satellites were made during the 1968 spring-summer season. The path length differences were determined by the high-angle and low-angle methods previously described. The results of the measurements on 23 total passes of four different satellites are plotted in Fig. 3.

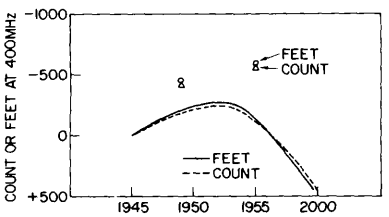

(a) Satellite 2754 or 1967 034A; 6-24-68; 1943-2000Z; CA (closest approach), 44°; rise az., 9°; set az., 164°

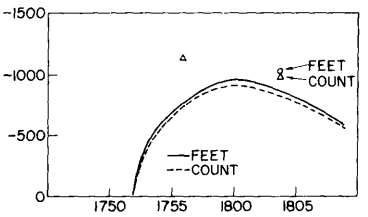

(b) Satellite 2807 or 1967 048A; 5-10-68; 1751-1804Z; CA, 70°; rise az., 183°; set az., 357°

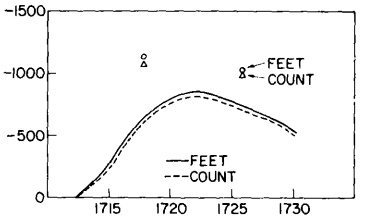

(c) Satellite 2807 or 1967 048A; 5-13-68; 1713-1731Z; CA, 73°; rise az., 170°; set az., 1°

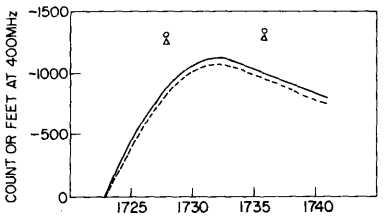

(d) Satellite 2807 or 1967 048A; 5-15-68; 1723-1741Z; CA, 81°; rise az., 179°; set az., 358°

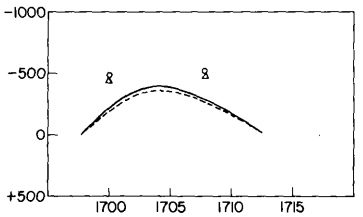

(e) Satellite 2807 or 1967 048A; 5-20-68; 1655-1705Z; CA, 87°; rise az., 175°; set az., 359°

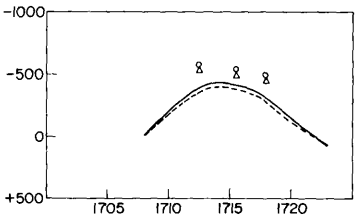

(f) Satellite 2807 or 1967 048A; 5-22-68; 1705-1723Z; CA, 68°; rise az., 184°; set az., 356°

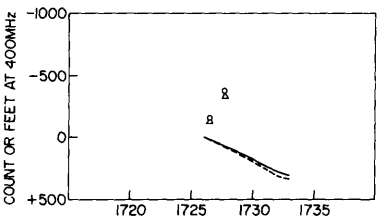

(g) Satellite 2807 or 1967 048A; 5-24-68; 1716-1733Z; CA, 49°; rise az., 195°; set az., 352°

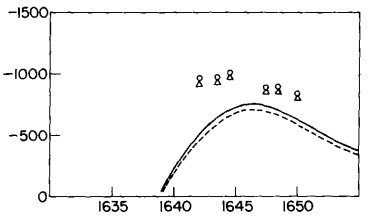

(h) Satellite 2807 or 1967 048A; 5-27-68; 1637-1655Z; CA, 77°; rise az., 181°; set az., 357°

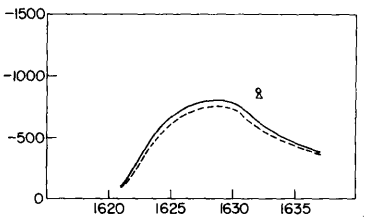

(i) Satellite 2807 or 1967 048A; 6-3-68; 1619-1637Z; CA, 64°; rise az., 186°; set az., 355°

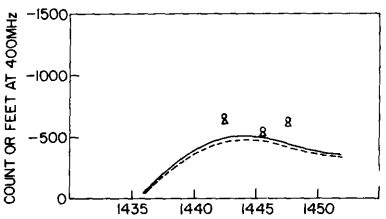

(j) Satellite 2807 or 1967 048A; 6-14-68; 1435-1452Z; CA, 46°; rise az., 157°; set az., 7°

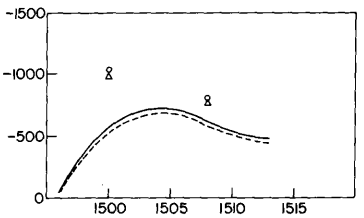

(k) Satellite 2807 or 1967 048A; 6-18-68; 1455-1512Z; CA, 87°; rise az., 175°; set az., 359°

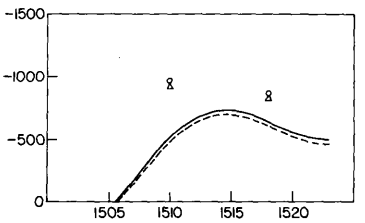

(l) Satellite 2807 or 1967 048A; 6-20-68; 1505-1523Z; CA, 68°; rise az., 184°; set az., 356°

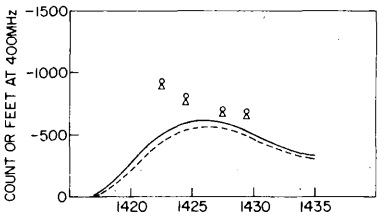

(m) Satellite 2807 or 1967 048A; 6-21-68; 1417-1435Z; CA, 56°; rise az., 162°; set az., 4°

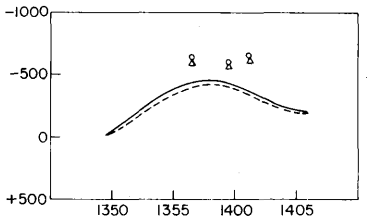

(n) Satellite 2807 or 1967 048A; 6-26-68; 1349-1406Z; CA, 49°; rise az., 190°; set az., 354°

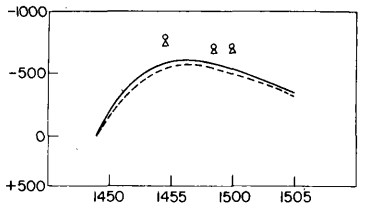

(o) Satellite 2807 or 1967 048A; 6-27-68; 1448-1505Z; CA, 56°; rise az., 190°; set az., 354°

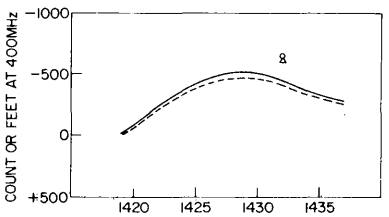

(p) Satellite 2807 or 1967 048A; 7-2-68; 1419-1437Z; CA, 65°; rise az., 186°; set az., 355°

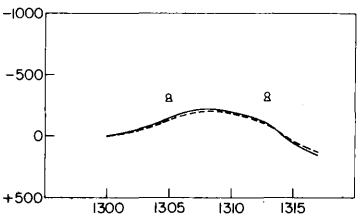

(q) Satellite 2965 or 1967 092A; 5-13-68; 1300-1318Z; CA, 77°; rise az., 2°; set az., 179°

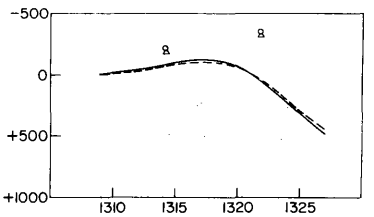

(r) Satellite 2965 or 1967 092A; 5-17-68; 1309-1327Z; CA, 68°; rise az., 358°; set az., 192°

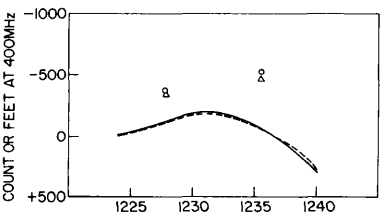

(s) Satellite 2965 or 1967 092A; 5-20-68; 1223-1240Z; CA, 67°; rise az., 4°; set az., 175°

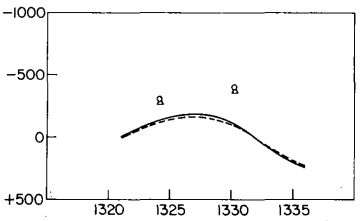

(t) Satellite 2965 or 1967 092A; 5-21-68; 1319-1336Z; CA, 42°; rise az., 352°; set az., 205°

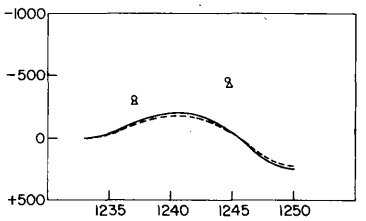

(u) Satellite 2965 or 1967 092A; 5-24-68; 1232-1250Z; CA, 78°; rise az., 8°; set az., 188°

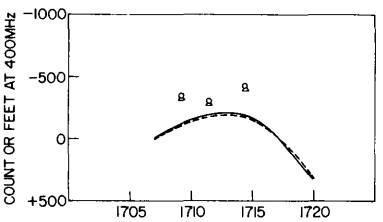

(v) Satellite 3133 or 1968 012A; 6-21-68; 1704-1722Z; CA, 51°; rise az., 8°; set az., 168°

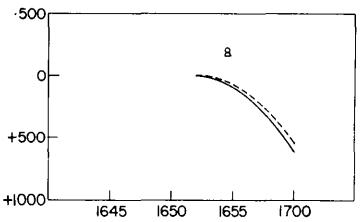

(w) Satellite 3133 or 1968 012A; 6-28-68; 1644-1701Z; CA, 57°; rise az., 7°; set az., 170°

Fig. 3 - Data for 23 satellite passes giving the approximate range errors caused by ionospheric irregularities. Note that the delay ΔL, as indicated in (a), is the difference between the particular curve and the zero offset value indicated by the points above the curve. The zero offset data points fail to fall on a horizontal line because of measurement errors.

Each graph shows delay in terms of feet at 400 MHz vs time similar to the presentation of Fig. A8 in the appendix. The zero offset (zero bias) values are shown by data points above where data were taken to calculate them. Each satellite is identified by two numbering systems, for example, 1967-048A (NASA) and 2807 (SPADATS). Each subtitle gives the rise and set times, rise and set azimuth angles, and closest approach (CA) elevation angles as observed from NRL.

The direction of orbit can be determined by noting the azimuth angles of rise and set. The dissymmetry of the curves show a greater rise length for a south-to-north pass or vice versa, showing the expected denser ionospheric conditions lying south of NRL. The approximate maximum range (labeled in Fig. 3a) is the difference between the lowest foot count (rise or set) and an approximate zero offset. The range in zero offset values indicates the possible error inherent in the system for measuring ΔL. This range is also portrayed in Fig. A8.

REFERENCES

1. Budden, K.G., "The Waveguide Mode Theory of Wave Propagation," Prentice-Hall, Aug. 1960, p. 13

2. Willman, J.F., and Tucker, A.J., "Accuracy of Satellite Doppler Data for Ionospheric Study, Navigation, and Geodesy," J. Geophys. Research, Space Phys. 73(No. 1):389-390 (Jan. 1, 1968)

3. "Interim Scientific Report, Phase Difference Navigation Satellite Report," RCA (DEP), Moorestown, N.J., Contract NAS-12-509 for ERC-NASA Cambridge, Mass., June 1967

   a. Sect. 6.3.2
   b. pp. 6-38
   c. Figs. 6-13, pp. 6-36
   d. pp. 6-59
   e. pp. 6-38

4. Ron, W.J., Garriatt, O.K., DeMendonca, F., and DaRosa, A.V., "Comments on Local Electron Concentration Determination from Doppler Measurements of Satellite Radio Beacons," J. Geophys. Research, Space Phys. 73(No. 3):1102 (Feb. 1, 1968)

5. Buisson, J.A., III, and DeVezin, H.G., Jr., "Look-Angle Prediction Technique for Artificial Earth Satellites," NRL Report 6351, Dec. 30, 1965

Appendix A

CALCULATIONS OF RANGE ERROR BY THE LOW-ANGLE AND HIGH-ANGLE METHODS

Two methods are described for determining the range error between satellite and ground observer due to the ionospheric effect. One is the low-angle method for ϕ valued around 22.5° to 32.5°. The second method is the high-angle method which uses the approximation $Q = \csc \phi$ and which is good for $\phi > 45°$. It is a much simpler method than the first.

Included are samples of typical worksheets demonstrating the methods of calculating the data obtained from a typical recording of ionospheric correction signal (f_{mix}) from an SRN/9 receiver tuned to a Transit satellite. Also included is a typical satellite prediction sheet and some specially prepared graphs to aid in the rapid evaluation of some functions.

LOW-ANGLE METHOD

The worksheet sample shown in Fig. A1 demonstrates the order of calculation with a definition of the steps and gives the numerical values connected with each step for the particular satellite pass used.

The data from the predictions (Fig. A2) are tabulated to include the range ϕ = 22.5° to 32.5° for both rise and set. For both rise and set a linear approximation is used to find the times ($T_{22.5°}$, $T_{27.5°}$, and $T_{32.5°}$) the satellite is at the elevation angles 22.5°, 27.5°, and 32.5°. Using these times and the recorded correction signal data from the SRN/9 receiver (Fig. A3 shows a portion of the recorded signals during set) the counts ($C_{22.5°}$, $C_{27.5°}$, and $C_{32.5°}$) are found for both rise and set by taking the difference in the readings of the two counters as described in the test. The sign of the count is determined by considering the rate of change of count to be negative before closest approach of the satellite (CA). From the recorded data, the differences in count $C_{22.5°} - C_{27.5°}$ and $C_{27.5°} - C_{32.5°}$ are found to one-tenth of a count accuracy and logged as designated on the sample worksheets. By averaging these count groups, $C_{25°}$ and $C_{30°}$ are found. K is the ratio of the slope $C_{22.5°} - C_{27.5°}$ to the slope $C_{27.5°} - C_{32.5°}$. Figure A4 was prepared for the easy evaluation of the thin shell height $\bar{h}$ vs $K_{25° - 30°}$. The values of $Q(\bar{h}, 25°)$, $Q(\bar{h}, 30°)$, and $Q(\bar{h}, 25°) - Q(\bar{h}, 30°)$ are easily found from Figs. A5 and A6. By the use of the formulas indicated on the work sheets, $N_T b/\omega^2$, $\Delta L_{25°}$, and $\Delta L_{30°}$, the zero offset, and the zero offset differences are found.

HIGH-ANGLE METHOD

Similar to the example of the first method, the sample worksheets of Fig. A7 is provided. The angles ϕ_1 and ϕ_2 and the times t_1 and t_2 obtained from the predictions (Fig. A2) are logged on the worksheet. Likewise the counts c_1 and c_2, obtained from the output of the SRN/9 receiver (Fig. A3) are listed on the worksheets. From this the average time and average angle are derived for the interval. Likewise the average count is determined. Using the tangent of the average angle $\bar{\phi}$, ΔL is obtained from $(\Delta c/\Delta\phi \tan \bar{\phi}$

in terms of count. The zero offset in counts is the average count $\bar{c}$ minus ΔL. The data were left in the form of counts to be equated to linear dimensions based on the chosen linear unit per count for the frequency as shown in Fig. A8.

IONOSPHERIC DELAY VS TIME

Figure A8 shows typical ionosphere delay vs time for the particular satellite pass used throughout the example. This is applicable to the data obtained by both methods. The zero offsets are shown as points at positions along the abscissa to show the areas of data from which they were calculated.

Sat. No.: 2807 Date: May 27, 1967
Time: 1637-1655 Max. Elev.: 77°

	Rise		Set		
	Time	Elev.	Time		Elev.
Values from predictions	1641	19.4672	1649		37.1856
	1642	26.6930	1650		27.6372
	1643	36.0649	1651		20.2941
Linear approximations between prediction points	Minutes	Seconds			
$T_{22.5°}$	1641	25.2	1650		42.0
$T_{27.5°}$	1642	05.2	1650		01.1
$T_{32.5°}$	1642	37.2	1649		29.4
$C_{22.5°}$	-376	From data (± 1 count)	-7/3 + 164	=	-549
$C_{27.5°}$	-450		-7/3 + 127	=	-586
$C_{32.5°}$	-503		-7/3 + 100	=	-613
$C_{22.5°} - C_{27.5°}$	76.4	From data (± 0.1 count)	36.3		
$C_{27.5°} - C_{32.5°}$	56.3		26.5		
$C_{25°}$	-413	$\frac{C_{22.5°} + C_{27.5°}}{2}$	-567.5		
$C_{30°}$	-476.5	$\frac{C_{27.5°} + C_{32.5°}}{2}$	-599.5		
K	1.357	$\frac{C_{22.5°} - C_{27.5°}}{C_{27.5°} - C_{32.5°}}$	1.370		
h	115	From $\bar{h}$ vs K plot	103		
$Q(\bar{h}, 25°)$	2.193	From $Q(\bar{h}, 25°)$ vs K plot	2.215		
$Q(\bar{h}, 30°)$	1.899	From $Q(\bar{h}, 30°)$ vs K plot	1.912		
$Q(\bar{h}, 25°) - (\bar{h}, 30°)$	0.292	From $Q(h, 25°) - Q(h, 30°)$ vs K plot	0.301		$\frac{(C_{22.5°} - C_{27.5°}) + (C_{27.5°} - C_{32.5°})}{2[Q(\bar{h}, 25°) - Q(\bar{h}, 30°)]}$
$N_t b/\omega^2$ (counts	$\frac{132.7}{2(0.292)} = 227$		$\frac{62.8}{2(0.301)} = 104$		
$\Delta L_{25°}$ (counts)	498	$\frac{N_t b}{W^2} \times Q(\bar{h}, 25°)$	230		
$\Delta L_{30°}$ (counts)	431	$\frac{N_t b}{W^2} \times Q(\bar{h}, 30°)$	199		
Zero Offset (counts)	-907.5	$-\Delta L_{30°} + C_{30°}$	-798.5		
Zero Offset Difference (counts)	109.0	|Rise zero offset - Set zero offset|			

1 count = 1.0737 ft at 400 MHz
1 count = 7.6352 ft at 150 MHz

Fig. A1 - Explanatory worksheet sample to demonstrate the low-angle method of calculating range error

DATE	HR	MIN	SECONDS	AZIMUTH	ELEV	RANGE	RANGERT	DOPPLER
52768	16	37	0.0	180.8299	1.0320	3777.339	-6.202	8.937
52768	16	38	0.0	181.4014	4.6997	3405.844	-6.177	8.900
52768	16	39	0.0	182.1062	8.8498	3036.842	-6.117	8.814
52768	16	40	0.0	183.0055	13.6739	2672.867	-6.005	8.654
52768	16	41	0.0	184.2092	19.4672	2317.802	-5.813	8.377
52768	16	42	0.0	185.9328	26.6930	1977.950	-5.486	7.906
52768	16	43	0.0	188.6653	36.0649	1664.125	-4.923	7.094
52768	16	44	0.0	193.7055	48.5347	1395.356	-3.948	5.688
52768	16	45	0.0	206.9060	64.5024	1203.346	-2.332	3.360
52768	16	46	0.0	294.3243	77.3161	1128.667	-0.085	0.123
52768	16	47	0.0	328.2996	66.0013	1193.714	2.189	-3.154
52768	16	48	0.0	342.9639	49.8927	1378.586	3.852	-5.551
52768	16	49	0.0	348.4069	37.1856	1642.764	4.863	-7.007
52768	16	50	0.0	351.3908	27.6372	1953.589	5.445	-7.846
52768	16	51	0.0	353.2341	20.2941	2291.277	5.781	-8.331
52768	16	52	0.0	354.5260	14.4239	2644.586	5.978	-8.614
52768	16	53	0.0	355.5766	9.5492	3006.984	6.091	-8.777
52768	16	54	0.0	356.4118	5.3656	3374.470	6.151	-8.864
52768	16	55	0.0	357.1265	1.6759	3744.440	6.176	-8.900

Fig. A2 - Satellite predictions for satellite 2807 (1967 048A); longitude, 77.0248972°; latitude, 38.820208°; height above sea level, 0.01108 mi; doppler frequency, 400 MHz

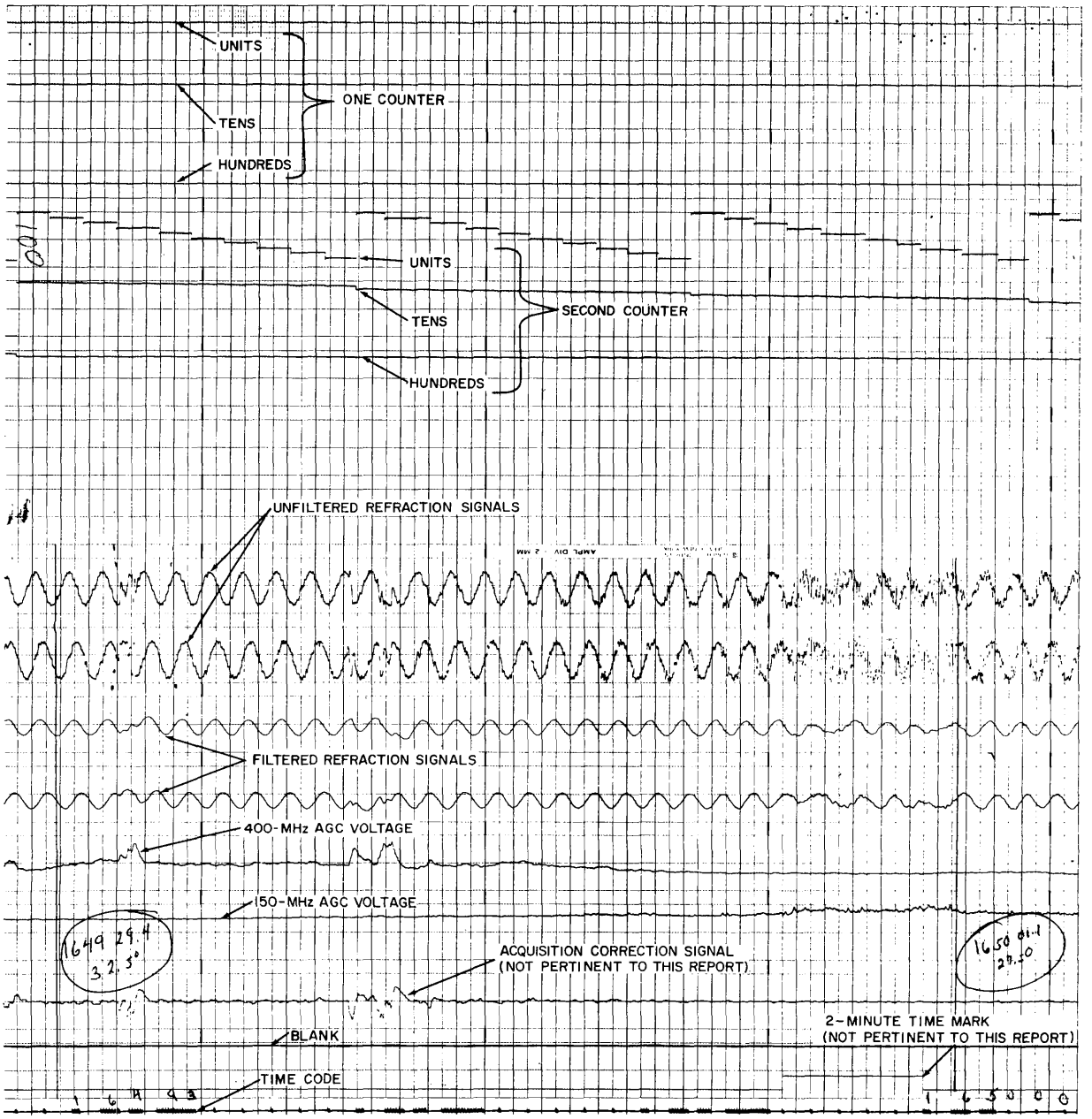

Fig. A3 - A portion of a recording of the ionospheric correction signal (f_{mix}) of a Transit satellite from an SRN/9 receiver

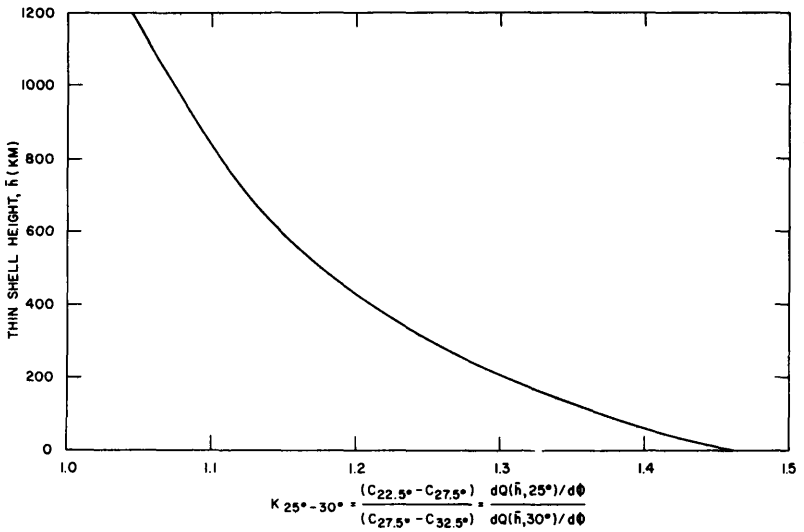

Fig. A4 - Thin shell height plotted against $K_{25°-30°}$ for use with the worksheet shown in Fig. A1

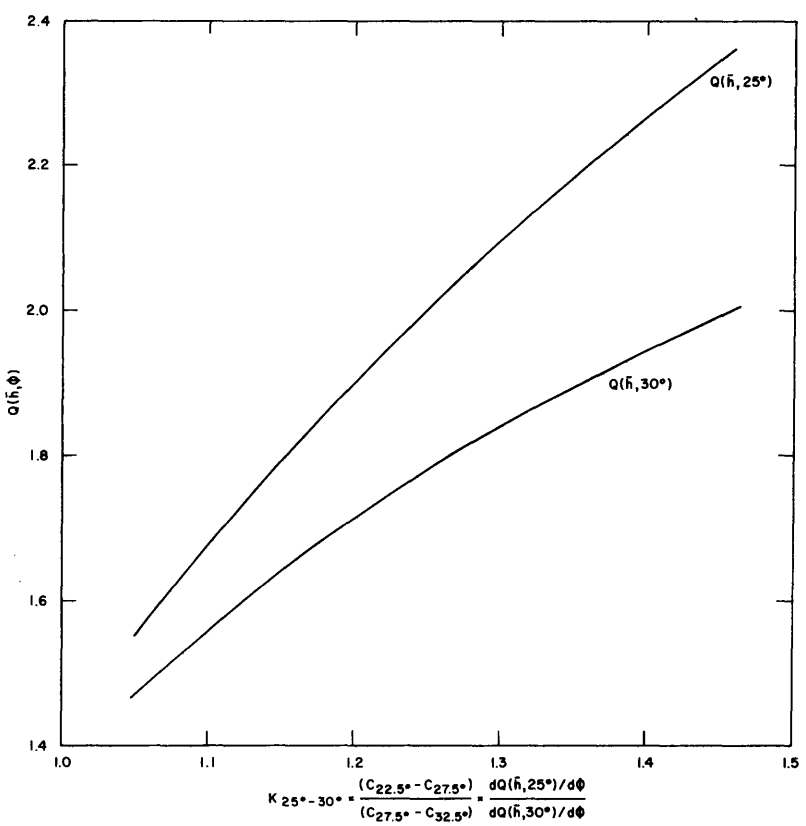

Fig. A5 - Graph prepared for use with the worksheet shown in Fig. A1

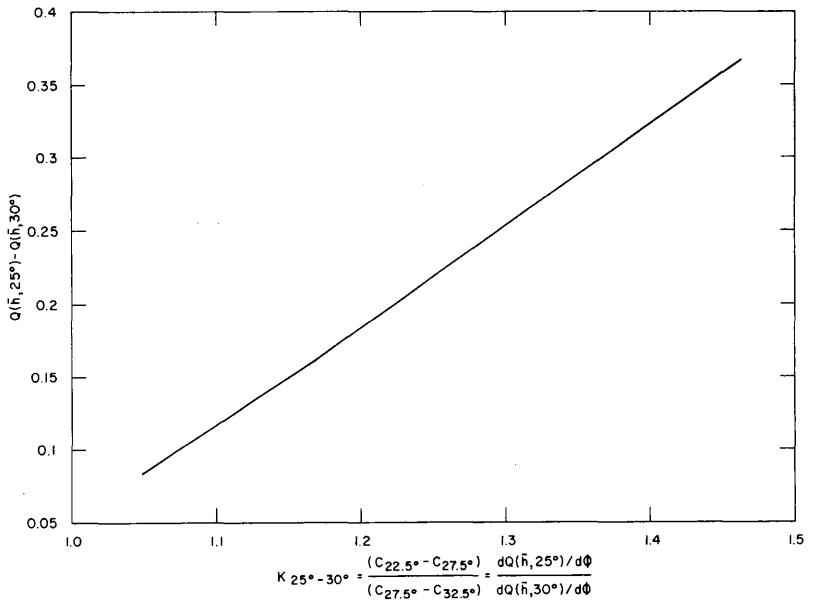

Fig. A6 - Values for the worksheet shown in Fig. A1

Date: 5-27-68
Time: Z1637-1655
Sat.: 2807

From predictions ϕ_1	36.0649	48.5347	66.0013	49.8927
ϕ_2	48.5347	64.5024	49.8927	37.1856
$\Delta\phi$	12.4698	15.9677	-16.1086	-12.7071
$(\phi_1 + \phi_2)/2$ $\bar{\phi}$	42.2998	56.5185	57.9470	43.5392
t_1	1643	1644	1647	1648
From predictions t_2	1644	1645	1648	1649
Δt	1 min	1 min	1 min	1 min
$(t_1 + t_2)/2$ $\bar{t}$	1643 30	1644 30	1647 30	1648 30
From data counts c_1	-540	-623	-708	-679
c_2	-623	-682	-679	-635
Δc	-83	-59	29	44
$(c_1 + c_2)/2$ counts $\bar{c}$	-581	-652	-694	-657
$\tan \bar{\phi}$	0.90993	1.5118	1.5972	0.95007
ΔL	347	320	165	188
Zero Offset	928	972	859	845

$(57.3°/\text{rad})\frac{\Delta c}{\Delta \phi} \tan \phi$ counts

$|\bar{c} - \Delta L|$ counts

Fig. A7 - Explanatory worksheet sample to demonstrate the high-angle method of calculating range error

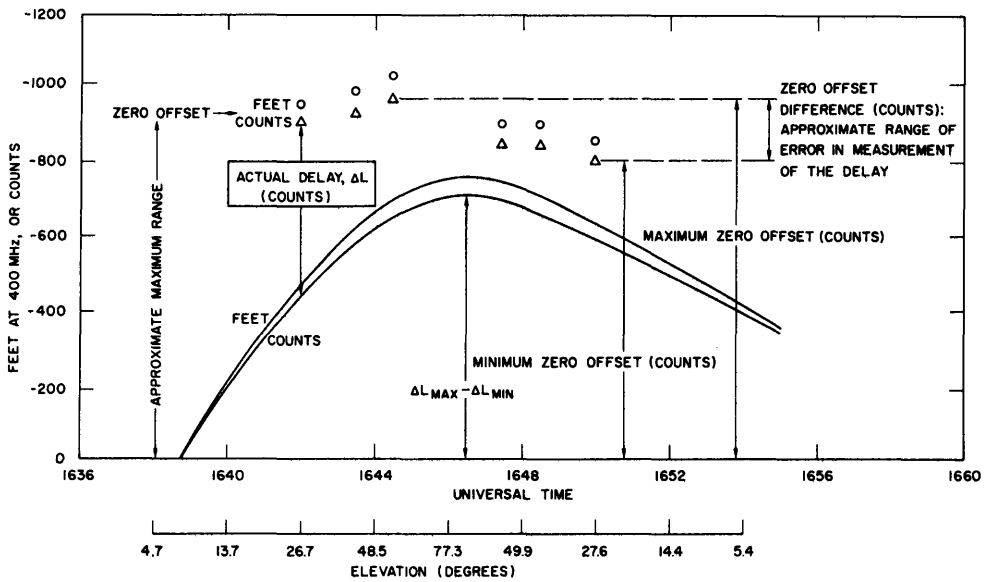

Fig. A8 - Calculated range error data for a typical satellite pass based on the preceding appendix figures. Note that the range error or actual delay is not given directly by the curve but by the difference between the curve and the zero offset value. Note further that the zero offset value, which should be a single horizontal line, is indicated by points over a range of values, which is a measure of errors in the measurements of the delay. The explanatory labels refer to the count values; similar labels would apply to the values in terms of feet of delay. Conversion from counts to distance is as follows: 1 count = 1.0737 ft (the curve shown) or 0.3273 m at 400 MHz and 1 count = 7.6352 ft or 2.3275 m at 150 MHz.

Security Classification

DOCUMENT CONTROL DATA - R & D

(Security classification of title, body of abstract and indexing annotation must be entered when the overall report is classified)

1. ORIGINATING ACTIVITY *(Corporate author)* Naval Research Laboratory Washington, D.C. 20390	2a. REPORT SECURITY CLASSIFICATION Unclassified 2b. GROUP

3. REPORT TITLE

IONOSPHERE PROPAGATION DELAY MEASUREMENT TECHNIQUES USING DUAL PHASE COHERENT DOPPLER FREQUENCIES AND A THIN SHELL MODEL

4. DESCRIPTIVE NOTES *(Type of report and inclusive dates)*

An interim report on a continuing problem.

5. AUTHOR(S) *(First name, middle initial, last name)*

G. Paul Landis and Louis D. Breetz

6. REPORT DATE April 8, 1969	7a. TOTAL NO. OF PAGES 24	7b. NO. OF REFS 5
8a. CONTRACT OR GRANT NO. NRL Problem R04-16 b. PROJECT NO. A37-538-002/652-1/F019-01-01 c. d.	9a. ORIGINATOR'S REPORT NUMBER(S) NRL Report 6861 9b. OTHER REPORT NO(S) *(Any other numbers that may be assigned this report)*	

10. DISTRIBUTION STATEMENT

This document has been approved for public release and sale; its distribution is unlimited.

11. SUPPLEMENTARY NOTES	12. SPONSORING MILITARY ACTIVITY Department of the Navy (Naval Air Systems Command), Washington, D.C. 20360

13. ABSTRACT

A theoretical approach was made to developing a technique for approximating the time error of a signal from a satellite caused by free electrons reducing the electromagnetic propagation speed. The development involved the use of the Transit satellites' dual frequency transmissions at 400 and 150 MHz, the AN/SRN-9 receiver, and a knowledge of the orbital location of the satellite. The technique gives a reasonably close delay measurement for a given satellite at a given time under a given ionospheric condition.

DD FORM 1 NOV 65 1473 (PAGE 1)

S/N 0101-807-6801

Security Classification

Security Classification

14. KEY WORDS	LINK A ROLE	LINK A WT	LINK B ROLE	LINK B WT	LINK C ROLE	LINK C WT
Navigation						
Navigation satellites						
Transit satellite						
Timation satellite						
Time measurement						
Time transfer						
Measurement						
Ionosphere						
Analysis (mathematics)						
Electromagnetic radiation						
Electromagnetic wave transmission						
Snell's law						
Refraction						
Velocity						
Distance						
Errors						

DD FORM 1 NOV 65 1473 (BACK)
(PAGE 2)

Security Classification